Journal of Molecular Graphics and Modelling 62 (2015) 294–302

Contents lists available at ScienceDirect

Journal of Molecular Graphics and Modelling

journal homepage: www.elsevier.com/locate/JMGM

Insight into the relationship between structure and magnetic properties in icosahedral Fe_nPt_{55-n} (n = 0–55) nanoparticles: DFT approach

Minghua Zhang, Ning Wang, Yongpeng Yang, Shiping Huang*

State Key Laboratory of Organic–Inorganic Composites, Beijing University of Chemical Technology, Beijing 100029, China

ARTICLE INFO

Article history:
Received 25 June 2015
Received in revised form 17 October 2015
Accepted 19 October 2015
Available online 26 October 2015

Keyword:
Fe_nPt_{55-n} nanoparticles
Structure
Electronic properties
Magnetic properties
Density functional theory

ABSTRACT

Structural, electronic and magnetic properties of Fe_nPt_{55-n} nanoparticles have been systematically studied based on the density functional theory. Firstly, the results show that surface Fe fraction has the same change tendency with excess energy and the nanoparticles have high stability when surface Fe fraction is small and excess energy is low. Secondly, analysis of Bader charge illustrates that the charge transfer reaches the maximum with Pt/Fe atomic ratio of 1:1. Thirdly, total magnetic moments of Fe_nPt_{55-n} nanoparticles increase with the increasing of Fe composition. Pt atom at the center site has promotion effect on the total magnetic moments of Fe_nPt_{55-n} nanoparticles, while Pt atom at the sublayer or outmost layer has inhibition effect. For the atomic magnetic moment, Fe atom occupying the edge of vertex in the second shell site (the center site) has maximum (minimum) atomic magnetic moment.

1. Introduction

Bimetallic transition-metal (TM) nanoparticles (NPs) have been widely studied not only because of their unique optical [1–4], electronic [5,6], and catalytic [7–18] properties that are different from the corresponding monometallic nanoparticles, but also due to the tunable properties achieved by changing the size, shape, and composition that may promote bimetallic transition-metal nanoparticles being applied to many fields [19–21]. Among all bimetallic TM systems, FePt nanoparticles have received enormous attention, since FePt nanoparticles present good chemical properties, such as catalytic activities toward the oxygen reduction reaction (ORR) [6,7], and show some physical properties, e.g., high saturation magnetization [22], high magnetocrystalline anisotropy [23].

Great efforts have been made to explore the ORR activity of FePt nanoparticles. Carbon-supported Pt and Pt–M (M = Fe, Co, and Cr) alloy catalysts were prepared by a polyol reduction method. ORR activity of Pt–M (M = Fe, Co, and Cr) alloy catalysts were found to be ~1.5 times higher than those of Pt/C catalysts for the direct ethanol fuel cell. The enhancement of ORR activity is due to the inhibition of formation of (hydr) oxy species on the Pt surface by the presence of alloying element [24]. Shukal et al. prepared carbon-supported Pt and carbon-supported Pt–Fe (1:1 atomic ratio) alloy catalysts by an alloying method and found that Pt–Fe/C alloy has a better ORR activity than Pt/C catalyst for solid–polymer–electrolyte direct methanol fuel cells [25]. The results of XPS and XAS suggest that there are two reasons that contribute to the enhancement of ORR activity. On the one hand, Pt–Fe/C catalyst contains a higher proportion of platinum active sites in relation to Pt/C catalyst. On the other hand, compared with Pt/C catalyst, there is a distinctly different nearest neighbour environment in Pt–Fe/C catalyst where the nearest sites are occupied by Fe atoms, which helps to scavenge impurities from the neighbouring active platinum sites. Fe_xPt_{1-x} catalysts with various Pt-to-Fe mole ratios and tunable physical properties were synthesized by Huang et al. [26]. They discussed the effects of unfilled d states, the alloying extent of Pt and Fe, and the compositions on ORR activities. DFT calculations revealed that Fe atom transfers charge to Pt atom when the Fe 3*d* and Pt 5*d* orbitals undergo hybridization, and the extent of charge transfer is dependent on the magnitude of alloying in FePt nanoparticles. Electrochemical analysis provided direct evidence that the alloying extent strongly influences the catalytic activity of ORR. The combined XAS and DFT results indicated that the Pt_1Fe_1/C catalyst possesses higher alloying of Pt and Fe with a few unfilled d states, owns a higher electron transfer from Fe to Pt and has the higher ORR activities than Pt_1Fe_3/C, Pt_3Fe_1/C catalysts.

* Corresponding author. Fax: +86 10 64427616.
E-mail address: huangsp@mail.buct.edu.cn (S. Huang).

http://dx.doi.org/10.1016/j.jmgm.2015.10.010
1093-3263/

Many studies on magnetic properties of FePt nanoparticles have been performed. Experimentally, Green and Thanh [27] found that the amount of Fe precursor has a big influence on magnetic properties of FePt nanoparticles under Schlenk conditions. In addition, the FePt nanoparticles synthesized in an autoclave have higher Fe content and crystallinity than those prepared on a Schlenk line. Theoretically, the magnetic properties of $(FePt)_n$ ($n = 1–5$) nanoparticles were studied by DFT [28]. The calculated results indicated that the spin magnetic moment and the binding energy increase with the increasing of nanoparticle size, although the spin magnetic moment per (FePt) unit remains unaltered. With the increasing of nanoparticle size, the orbital and spin magnetic moments of Pt atoms slightly increase while those of Fe atoms decrease. Mokkath [29] studied the magnetic properties of Fe_mPt_n nanoparticles ($N = n + m$, $N \leq 19$) by spin-polarized density-functional calculations, and mainly discussed the effects of size and composition on the spin magnetic moment, orbital magnetic moment and the magnetic anisotropy energies. The calculated results indicated the magnetic properties of the pure Fe and Pt nanoparticles change dramatically with decreasing nanoparticles size. This is because the orbital magnetic moment is sensitive to the changes of the local coordination number. For Fe_mPt_n ($m + n = 13$, 19) nanoparticles, both the orbital magnetic moment and the magnetic anisotropy energies oscillatorily change with the increasing of nanoparticle size and composition, which are due to the substitutional nanoalloy that clearly enhances the orbital moments and boosts the magnetic anisotropy energies by lowering the overall cluster symmetry. Although the size and composition of nanoparticles have a significant influence on the magnetic properties, this characteristic is not well understood on atomic scale.

In this work, we carry out a study on the Fe_nPt_{55-n} nanoparticles based on the density functional theory. We mainly discuss structural, electronic, and magnetic properties of icosahedral Fe_nPt_{55-n} nanoparticles. First, a series of geometrical structures about icosahedral Fe_nPt_{55-n} nanoparticles with the Fe and Pt atoms randomly distributing are obtained. Then, we calculate excess energy to investigate the stabilities of the nanoparticles. Through the analysis of the difference charge density and Bader charge, we obtain that the charge is transferred from Fe atom to Pt atom. Finally, we analyze the variation of magnetic moment of Fe_nPt_{55-n} nanoparticles as a function of the number of Fe atoms and discuss the effect of Pt atoms on the total magnetic moment.

2. Computational methods

For the geometry optimizations, the spin-polarized density functional theory (DFT) calculations are performed using the CP2K [30] code in the Gaussian and plane waves (GPW) [31] formalism. The electronic exchange-correlation energy is calculated with the Perdewe–Beckee–Ernzerhof (PBE) [32] form of the generalized gradient approximation (GGA). The core electrons and nuclei are represented using the analytical dual-space pseudo-potential recommended by Goedecker, Teter and Hutter (GTH) [33], and the valence electrons are treated with a double-z valence basis set with one set of polarization functions, the DZVP basis set [34]. The plane-wave cut-off energy is set to 300 Ry in this study. The energy is converged to 1×10^{-5} Ha. The nanoparticle is placed in a $20 \times 20 \times 20$ Å^3 cubic box with periodic boundary condition, which ensures that the interaction of nanoparticle with its periodic image is negligible.

The electronic and magnetic properties calculations for the nanoparticles are performed based on Vienna *ab* initio Simulation Package (VASP) [35], adopting the projector augmented wave method (PAW) pseudopotentials. The density function is treated within the generalized gradient approximation (GGA), using the PBE [32]. The plane-wave cut off is set to be 300 eV. The residual force is less than 10^{-2} eV/Å and the total energy is converged to 10^{-5} eV/atom. The k-point mesh is generated by the Gamma centered method, which is used in the electronic and magnetic properties calculations. All calculations are performed under the condition of periodic boundary.

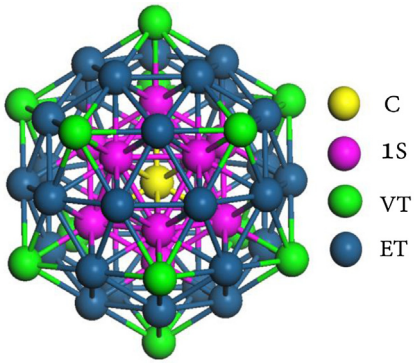

Fig. 1. Icosahedral structure (space group I_h) with 55 atoms. The atoms with different color show four nonequivalent sites, namely, the center site (C), the first shell site (1S), the top of vertex in the second shell site (VT), and the edge of vertex in the second shell site (ET). (For interpretation of the references to color in this figure legend, the reader is referred to the web version of this article.)

3. Result and discussion

3.1. Structure and stability

Among all nanoparticles structure model, the icosahedron (ICO) structure has been widely used to model transition-metal nanoparticles [36,37]. The nanoparticle with icosahedral structure has good stability, and can be synthesized by the experiment techniques. In addition, icosahedral structure has a quasi-spherical shape and a close-packed surface with 20 distorted (111)-like facets. This packing surface causes the high internal strain of the structure, which results in icosahedron structure favoring for small size [38]. Here we adopt three shells icosahedron model with 55 atoms, and the particles diameter is approximately 1 nm. Fig. 1 shows the icosahedron structure and four nonequivalent sites, namely, the center site (C), the first shell site (1S), the top of vertex in the second shell site (VT), and the edge of vertex in the second shell site (ET).

There are various mixing models for bimetallic nanoparticles, such as random alloy, cluster-in-cluster, core/shell, inverted core/shell [39]. In our work, we mainly pay attention to the randomly mixed Fe_nPt_{55-n} nanoparticles with the composition of Fe ranging from 0% to 100%. Special models are also investigated in our work, including the core/shell and inverted core/shell structures. For each composition, there is a great deal of isomers, we firstly generated six randomly icosahedral configurations at the ratio of Fe/Pt = 1:2, 1:1, 1.5:1($Fe_{19}Pt_{36}$, $Fe_{27}Pt_{28}$, $Fe_{33}Pt_{22}$), respectively. Then randomly icosahedral configurations are optimized and the energies are obtained. Some rules between the structure and energy are observed as follows: (i) the isomer with more Pt atoms in the surface has the low energy in the Table S1 in supplement materials; (ii) the isomer with more Pt atoms at VT site has the low energy presented in Table S2 in supplement materials; (iii) the isomer that Pt atoms at VT site occupy more surfaces has the low energy listed in Table S3 in supplement materials. Base on three factors, we obtain a series of configurations of Fe_nPt_{55-n} ($n = 0–55$) nanoparticles. Fig. 2 shows the configurations of Fe_nPt_{55-n} ($n = 0–55$) nanoparticles with different Fe composition. We find that Fe_nPt_{55-n} nanoparticles keep icosahedral configuration with slight distortion that Fe atoms in the surface tend to

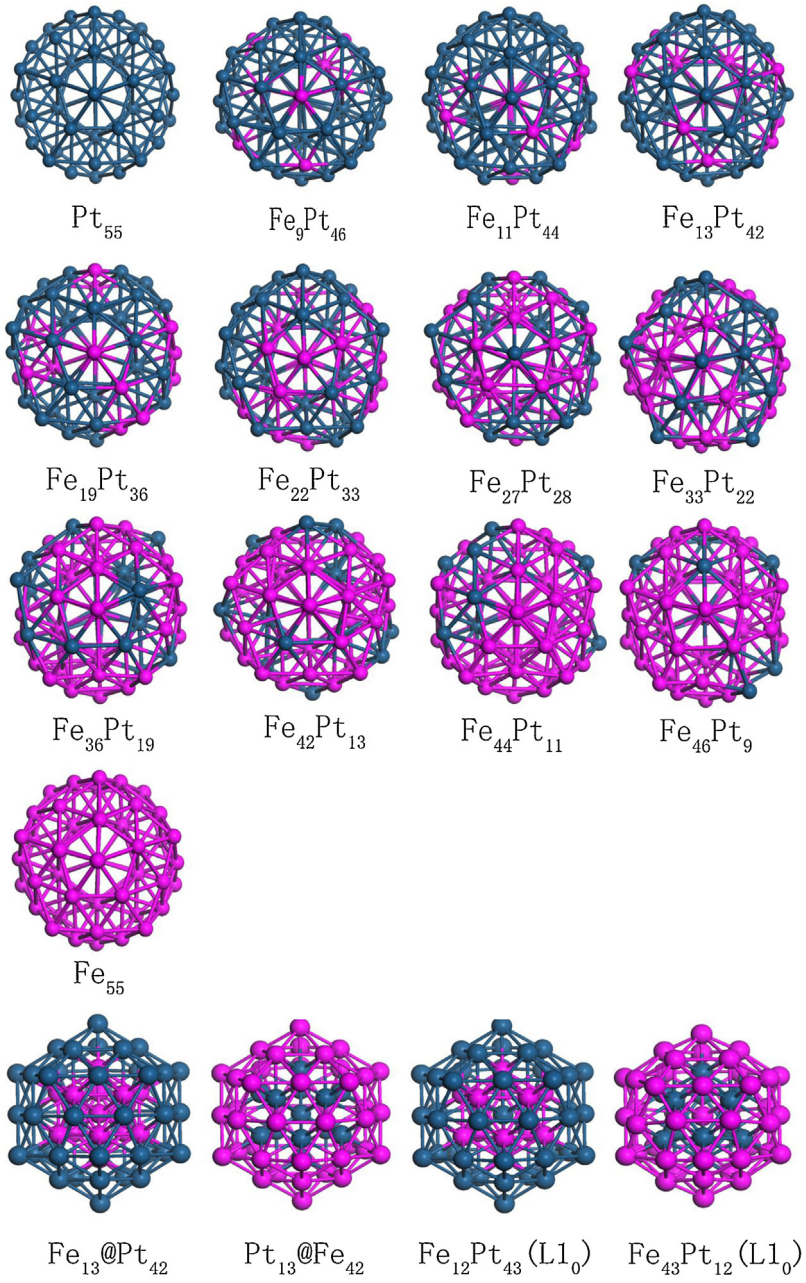

Fig. 2. Structures for Fe_nPt_{55-n} (n = 0–55) nanoparticles. Blue balls represent Pt atoms and pink balls represent Fe atoms. (For interpretation of the references to color in this figure legend, the reader is referred to the web version of this article.)

contract to internal, and the Pt atoms tend to expand to external at the temperature of 0 K under vacuum conditions. This distortion can be caused by the different atomic radius of Fe and Pt atom. The atomic radius of Fe atom is smaller than that of Pt atom, leading to the expanding and contracting of Pt atoms and Fe atoms.

The icosahedron structure consists of two parts, core and shell. In order to explore the distribution of the Fe and Pt atoms in the core and shell, we calculate the surface Fe and Pt fraction for randomly mixed Fe_nPt_{55-n} (n = 9–46) nanoparticles. The surface fraction can be defined as $F = M_{AS}/M_A$, where M_{AS} is the number of surface A atom, and the M_A is the total number of A atom. Fig. 3(a) shows that, in general, the surface Pt fraction is greater than surface Fe fraction in the Fe_nPt_{55-n} nanoparticles. This means that Pt atoms tend to occupy the surface site.

In order to explain this phenomenon, we calculate segregation energy. The segregation energy is the energy cost of transferring an impurity atom from the interior to the surface of a host cluster [40], which can be used as a standard to judge which site the atom prefers to occupy. For Fe_nPt_{55-n} nanoparticles, the segregation energy of Fe and Pt can be defined as:

$$E^{Fe}_{seg} = E_{Fe_{1VT}Pt_{54}} - E_{Fe_{1C}Pt_{54}} \quad (1)$$

$$E^{Pt}_{seg} = E_{Fe_{54}Pt_{1VT}} - E_{Fe_{54}Pt_{1C}} \quad (2)$$

where $E_{Fe_{1VT}Pt_{54}}$, $E_{Fe_{1C}Pt_{54}}$, $E_{Fe_{54}Pt_{1VT}}$, $E_{Fe_{54}Pt_{1C}}$represent the total energies of $Fe_{1VT}Pt_{54}$, $Fe_{1C}Pt_{54}$, $Fe_{54}Pt_{1VT}$ and $Fe_{54}Pt_{1C}$ (the subscript stands for the number of atoms and the occupied site, seen in Fig. 1) nanoparticles, respectively. The segregation energy is 2.60 eV for Fe and −3.45 eV for Pt. Considering that there are two sites in the surface (VT or ET), similarly, we calculate the total energy of $Fe_{1ET}Pt_{54}$ and $Fe_{54}Pt_{1ET}$ nanoparticles to analyze the segregation energy. A positive E_{seg} (0.83 eV) is also obtained for Fe and a neg-

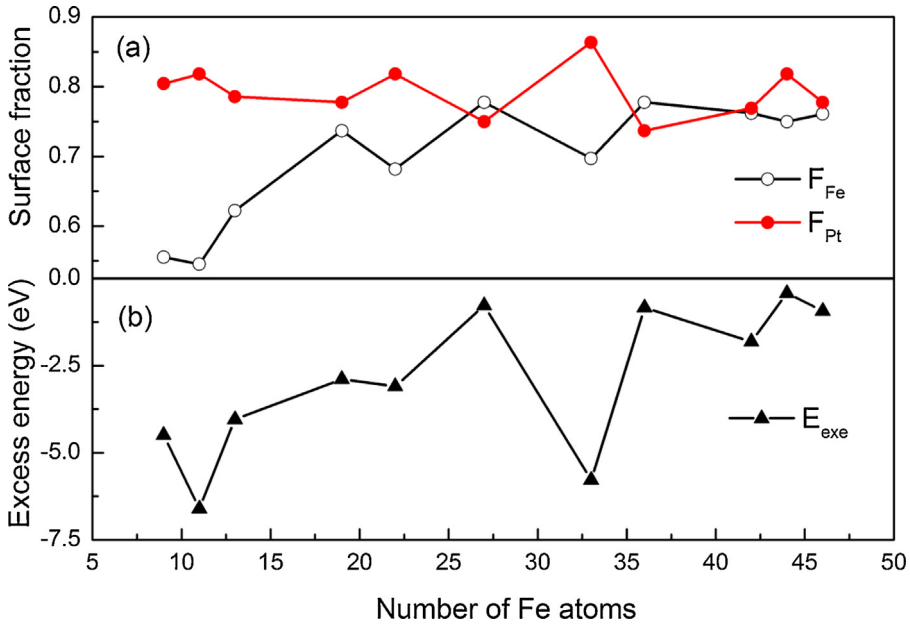

Fig. 3. (a) Surface fraction of Fe and Pt atoms as a function of the number of Fe atoms. (b) The excess energy varies with the number of Fe atom in the Fe_nPt_{55-n} nanoparticles.

ative E_{seg} (−3.12 eV) of Pt. The positive E_{seg} of Fe indicates that Fe atom tends to move inwards to occupy the center site. On the other hand, the negative E_{seg} of Pt proves that Pt atom prefers to move outwards to occupy the surface site. Therefore, this is the reason why more Pt atoms occupy the surface site in Fe_nPt_{55-n} nanoparticles.

To compare the relative stability of the different Fe composition of Fe_nPt_{55-n} nanoparticles, we calculate the excess energy (E_{exc}) as follows:

$$E_{exc} = E_{tot}^{Fe_nPt_{55-n}} - \frac{n}{55}E_{tot}^{Fe_{55}} - \frac{55-n}{55}E_{tot}^{Pt_{55}} \quad (3)$$

where $E_{tot}^{Fe_nPt_{55-n}}$,$E_{tot}^{Fe_{55}}$,$E_{tot}^{Pt_{55}}$ is the total energies of the Fe_nPt_{55-n}, Fe_{55}, and Pt_{55} nanoparticles, respectively. For randomly mixed nanoparticles, a negative value of E_{exc} indicates a tendency to form mixed nanoparticles, while the positive value characterizes segregation tendencies [41]. For randomly mixed Fe_nPt_{55-n} nanoparticles, the excess energies are negative as shown in Fig. 3(b), indicating that the randomly mixed Fe_nPt_{55-n} nanoparticles are relatively stable and energetically favorable in the thermodynamics.

Considering the surface Fe fraction may be one of the factors that affect stability of Fe_nPt_{55-n} nanoparticles, we investigate the relationship between the excess energy and the surface Fe fraction. We find that excess energy has the same change tendency with the surface Fe fraction, as shown in Fig. 3. When the surface Fe fraction is small, the excess energy is relatively low. For example, the surface Fe fraction is 0.54 in $Fe_{11}Pt_{44}$ nanoparticles, while the excess energy is −6.06 eV. In $Fe_{36}Pt_{19}$ nanoparticles with surface Fe fraction of 0.78, the excess energy is only −0.83 eV. To test this phenomenon, we calculate the excess energies of $Fe_{27}Pt_{28}$ nanoparticles with three different surface Fe fractions. When surface Fe fractions are 1, 0.78 and 0.52, the corresponding excess energies are 7.99, −0.77 and −13.33 eV, respectively. The excess energy is the lowest when the surface Fe fraction is 0.52. Therefore, we can conclude that Fe_nPt_{55-n} nanoparticles with smaller of the surface Fe fraction and lower of excess energy have higher stability.

In order to further clarify this characteristic, we calculate the surface Fe fraction and excess energy for four types of special structure: Fe_{13}@Pt_{42}, Pt_{13}@ Fe_{42}, $Fe_{12}Pt_{43}$ ($L1_0$), and $Fe_{43}Pt_{12}$ ($L1_0$) (seen in Fig. 2), and the results are shown in Table 1. We can find that when surface Fe fraction tends to be zero in Fe_{13}@Pt_{42} and $Fe_{12}Pt_{43}$ ($L1_0$) nanoparticles, the excess energies are very low, and the structures are relatively stable. However, when the most Fe atoms occupy the outmost layer in Fe_{42}@Pt_{13} and $Fe_{43}Pt_{12}$ ($L1_0$) nanoparticles, the excess energies are high and the structures are not stable. Therefore, it indicates that the Fe_{13}@Pt_{42} nanoparticle with the smallest surface Fe fraction and the lowest excess energy is the most stable structure among all the icosahedral Fe_nPt_{55-n} nanoparticles.

Table 1
Surface Fe fraction, the excess energy and the magnetic moment of the special Fe_nPt_{55-n} nanoparticles.

System	Fe_{13}@Pt_{42}	$Fe_{12}Pt_{43}(L1_0)$	$Fe_{43}Pt_{12}(L1_0)$	Fe_{42}@Pt_{13}
F_{Fe}	0	0	0.98	1
E_{exc}	−17.80	−14.49	28.11	28.59
$m_T(\mu_B)$	46.72	46.90	126.85	132.15

In order to analyze the structural characteristic of Fe_nPt_{55-n} nanoparticles, we calculate the partial coordination numbers N_{Fe-Fe}, N_{Fe-Pt}, N_{Pt-Fe} and N_{Pt-Pt}[42]. Fig. 4(a) shows the partial coordination numbers N_{Fe-Fe}, N_{Fe-Pt}, N_{Pt-Fe} and N_{Pt-Pt} in Fe_nPt_{55-n} nanoparticles. We find that the partial coordination numbers scale linearly with Fe composition, and the linear correlation coefficient is as high as 0.99. This behavior is similar to the ideal random alloy behavior [43]. This result indicates the structure of Fe_nPt_{55-n} nanoparticles adopt the random alloy model. In the random alloy, the ratio of the coordination numbers N_{Pt-Fe} and N_{Fe-Pt} is equal to the atomic radio of Fe/Pt. Therefore, we can determine the Fe composition by calculating the partial coordination numbers N_{Pt-Fe} and N_{Fe-Pt}. In addition, we also calculate the coordination numbers N_{FeM} ($N_{FeM} = N_{Fe-Fe} + N_{Fe-Pt}$) and N_{PtM} ($N_{PtM} = N_{Pt-Pt} + N_{Pt-Fe}$). The result exhibits that the coordination number N_{FeM} has the opposite change tendency with the excess energy, as shown in Fig. 4(b). Because the atoms at the surface have lower coordination number than the atoms in the core, the coordination number N_{FeM} is inversely proportion to the surface Fe fraction. The surface Fe fraction has the same change tendency with the excess energy, thus coordination number N_{FeM} is negatively correlated to the excess energy. When the excess energy is low and the coordination number N_{FeM} is large, the nanoparticle is relatively stable.

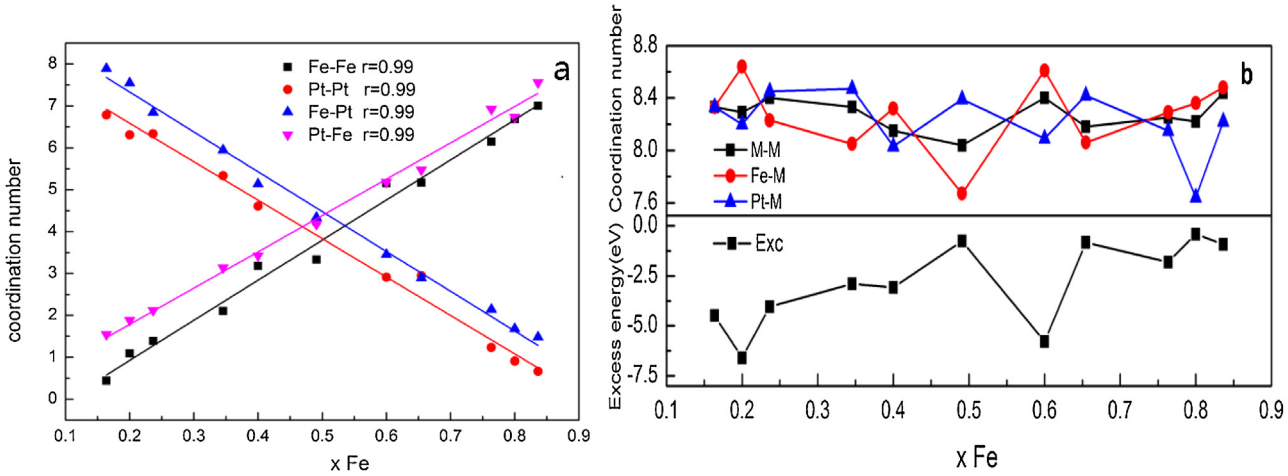

Fig. 4. (a) The particle coordination number of Fe–Fe, Fe–Pt, Pt–Fe, Pt–Pt as a function of Fe composition. (b) The particle coordination number of M–M, Pt–M, Fe–M and the excess energy as a function of Fe composition.

Table 2
Average bond lengths and average Bader charge in our calculation and in the EXAFS measurement[a] (The data in parentheses).

	Bond length (Å)			Transfers charges(e)	Bader charge(e)	
	Fe–Fe	Pt–Pt	Fe–Pt		Fe	Pt
Pt55	–	2.80	–	–	–	–
Fe_9Pt_{46}	2.15	2.85	2.60	6.56	0.73	−0.14
$Fe_{11}Pt_{44}$	2.50	2.75	2.65	7.72	0.70	−0.18
$Fe_{13}Pt_{42}$	2.55 (2.51)	2.80 (2.73)	2.60 (2.66)	8.79	0.68	−0.21
$Fe_{19}Pt_{36}$	2.60	2.85	2.65	11.34	0.60	−0.31
$Fe_{22}Pt_{33}$	2.50	2.70	2.65	11.11	0.51	−0.34
$Fe_{27}Pt_{28}$	2.55 (2.52)	2.85 (2.73)	2.65 (2.66)	11.65	0.43	−0.42
$Fe_{33}Pt_{22}$	2.45	2.80	2.55	11.20	0.34	−0.51
$Fe_{36}Pt_{19}$	2.40	2.85	2.55	10.46	0.29	−0.55
$Fe_{42}Pt_{13}$	2.45 (2.64)	2.75 (2.72)	2.55 (2.62)	8.95	0.21	−0.69
$Fe_{44}Pt_{11}$	2.40	2.85	2.50	7.57	0.17	−0.69
$Fe_{46}Pt_9$	2.40	2.70	2.50	6.74	0.15	−0.75
Fe55	2.45	–	–	-	–	–

[a] EXAFS measurement from Ref. [26].

The average bond length is another important structural parameter, which helps us to better understand structural characteristic of Fe_nPt_{55-n} nanoparticles. For Fe_nPt_{55-n} nanoparticles with different Fe composition, the average bond lengths of Pt–Pt, Fe–Fe, Fe–Pt are listed in Table 2. We compare the average bond lengths of Pt–Pt, Fe–Fe, Fe–Pt with the experimental value at the Fe and Pt atomic radio of 1:3, 1:1, 3:1, and find the error range from 0.41% to 7.30%. Thus, the calculated average bond lengths are consistent with the EXAFS measurements [26]. In addition, the order of the average bond length is as follows: Pt–Pt > Fe–Pt > Fe–Fe in the Fe_nPt_{55-n} nanoparticles, which is also in good agreement with the rule that the bond length of A-B at all concentration are located between A–A and B–B [43].

3.2. Electronic properties

In order to understand the charge distribution of Fe and Pt atoms in the Fe_nPt_{55-n} nanoparticles, we calculate the difference charge density. The difference charge density is defined as the difference between the charge density of the nanoparticles and atomic charge density of Fe and Pt atoms located in the same spatial coordinates as the nanoparticles [40]. Fig. 5 shows the difference charge density of $Fe_{12}Pt_{43}$ ($L1_0$) nanoparticle. The red color represents the charge accumulation and the blue color stands for the charge depletion. The accumulation of charge happens between Fe and Pt atoms and tends to encompass the Pt atom. The charge density around Pt atoms is larger than that around Fe atoms, which indicates that there exists the charge transfer between Fe and Pt atoms.

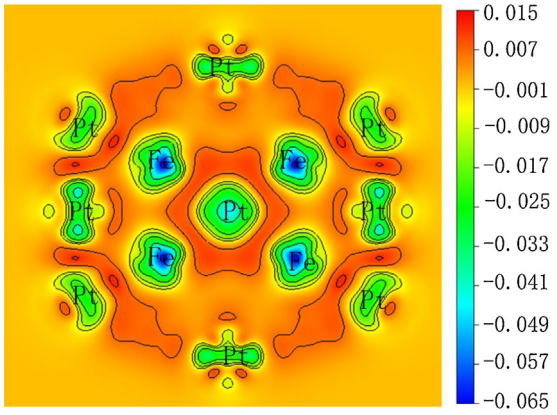

Fig. 5. The different charge density for $Fe_{12}Pt_{43}$ nanoparticle.

To analyze the charge distribution of Fe_nPt_{55-n} nanoparticles quantitatively, we calculate the average Bader charge of Fe and Pt atoms, presented in Table 2. Bader charge analysis reveals that Fe atoms are positively charged and Pt atoms are negatively charged. This indicates that Fe atom transfers charge to Pt atom. In addition, there is a similarly parabolic relationship between the extent of transferred charge and Fe composition that the extent of trans-

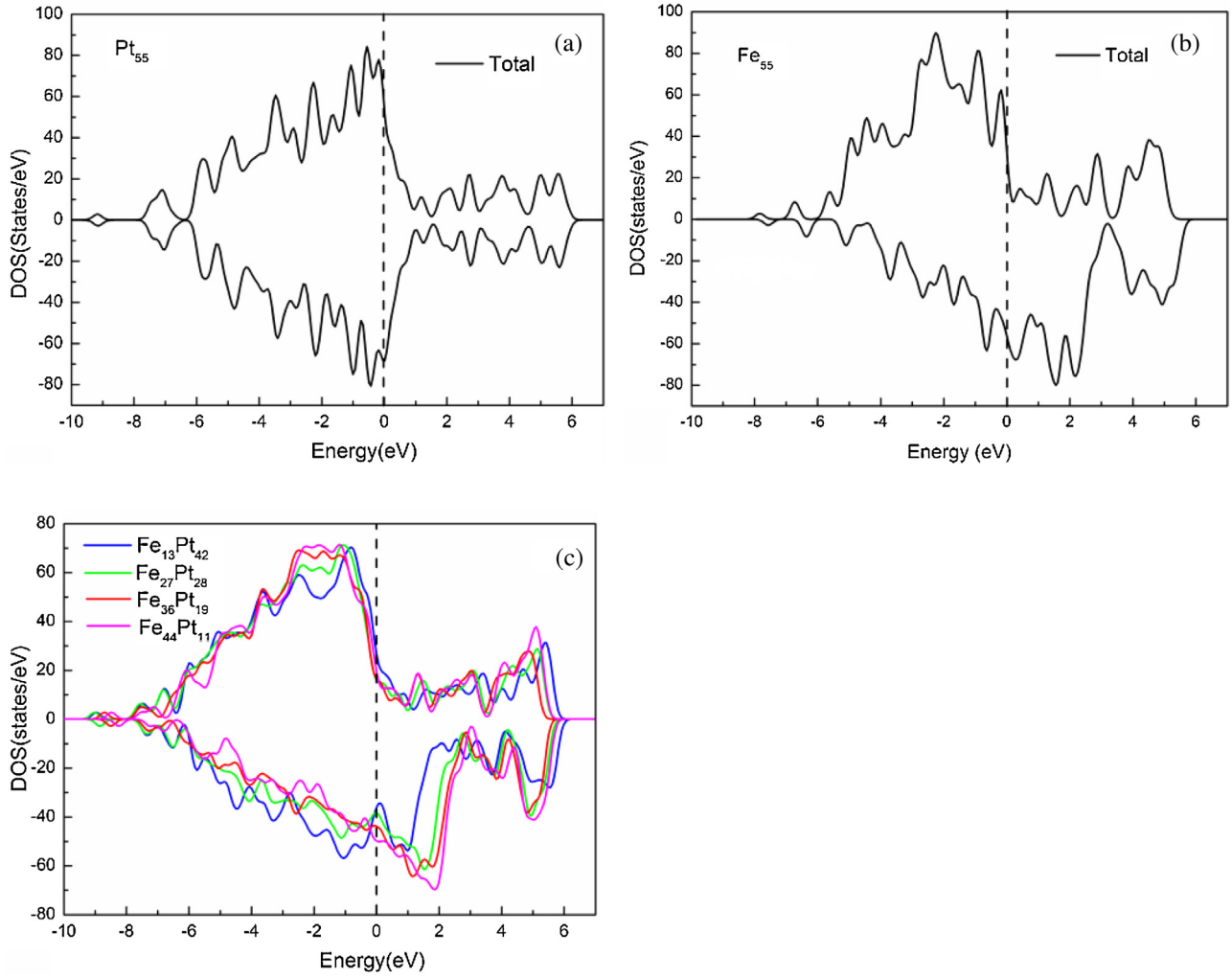

Fig. 6. The density of states for Fe_nPt_{55-n} nanoparticles. The Fermi level is set to zero. Positive (negative) values correspond to the majority (minority) spin.

Table 3
Total magnetic moments (m_T) and the average atomic magnetic moments of Fe and Pt atom in Fe_nPt_{55-n} nanoparticles.

Nanoparticles	$m_T(\mu_B)$	$Fe(\mu_B)$	$Pt(\mu_B)$
Pt55	7.97	-	0.14
Fe_9Pt_{46}	37.98	3.15	0.18
$Fe_{11}Pt_{44}$	45.25	3.07	0.22
$Fe_{13}Pt_{42}$	54.46	3.16	0.27
$Fe_{19}Pt_{36}$	72.38	3.05	0.33
$Fe_{22}Pt_{33}$	79.13	2.96	0.33
$Fe_{27}Pt_{28}$	91.53	2.89	0.35
$Fe_{33}Pt_{22}$	96.53	2.57	0.33
$Fe_{36}Pt_{19}$	112.58	2.62	0.38
$Fe_{42}Pt_{13}$	120.38	2.60	0.38
$Fe_{44}Pt_{11}$	125.18	2.61	0.39
$Fe_{46}Pt_9$	130.64	2.63	0.35
Fe55	145.29	2.50	–

ferred charge firstly increases and then monotonously decreases with the increasing of Fe composition except that the atomic ratio of Fe/Pt is 1:1.5. When the atomic ratio of Fe/Pt is 1:1, charge transfer reaches the maximum value. Therefore, composition may be one of factors that affect the extent of transferred charge.

3.3. Magnetic properties

Table 3 shows the average atomic magnetic moments of Fe and Pt, and the total magnetic moments of the Fe_nPt_{55-n} nanoparticles. We find that the total magnetic moments of Fe_nPt_{55-n} nanoparticles increase with the increasing of Fe composition. The average atomic magnetic moments of Fe in Fe_nPt_{55-n} nanoparticles gradually decrease to the minimum in $Fe_{33}Pt_{22}$ nanoparticles (2.57 μ_B), and then tend to be ~2.60 μ_B with the increasing of Fe composition. While the average atomic magnetic moments of Pt in Fe_nPt_{55-n} nanoparticles show an increasing tendency. The average atomic magnetic moments of Fe and Pt in Fe_nPt_{55-n} nanoparticles are larger than those in Fe_{55} and Pt_{55} nanoparticles. The study on the density of states (DOS) of Fe_nPt_{55-n} nanoparticles is helpful for understanding magnetic properties. The DOS of Fe_nPt_{55-n} nanoparticles is shown in Fig. 6. It is found that the states of spin up and spin down for Pt_{55} nanoparticle are nearly symmetrical, and the peaks for spin up and spin down mainly generate in the energy range from −6.0 to 1.0 eV, as shown in Fig. 6(a). While for Fe_{55} nanoparticle, the peaks for spin up and spin down mainly occur in the energy range from −6.0 to 0.0 eV and −4.0 to 3.0 eV, respectively, as shown in Fig. 6(b). This indicates that the exchange splitting occurs in the Fe_{55} nanoparticle. (The energy of electronic in the two kinds of spin bands (spin up band and spin down band) is different, which leads to the relative displacement between the two kinds of spin bands. The Fermi surface of one band increases and the Fermi surface of another band decreases. The splitting between two bands is defined as the exchange splitting [44].) Because of exchange splitting, Fe_{55} nanoparticle has the largest magnetic moment (145.29 μ_B). In randomly mixed Fe_nPt_{55-n} nanoparticles, with Fe composition

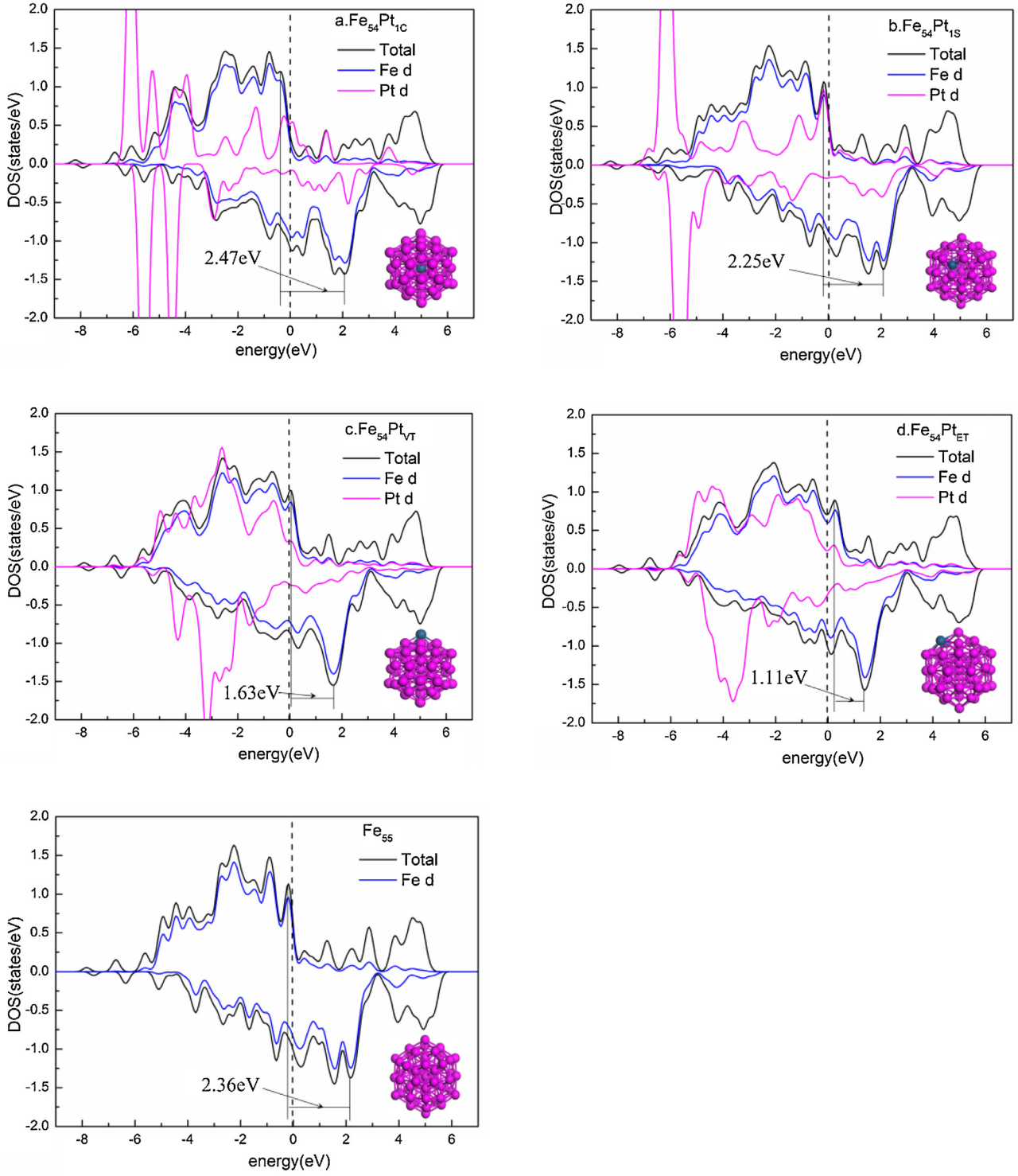

Fig. 7. The density of states of $Fe_{54}Pt_{1C}$, $Fe_{54}Pt_{1S}$, $Fe_{54}Pt_{1VT}$, $Fe_{54}Pt_{1ET}$ and Fe_{55} nanoparticles.

increasing, the peak at 0.0 to −2.0 eV for spin up shifts to lower energy level, while the peak at 0.0 to 2.0 eV for spin down moves away from Fermi surface, and shifts to a higher energy levels, as shown in Fig. 6(c). This characteristic implies that exchange splitting becomes more and more obvious with the increasing of Fe composition, leading to the increase of the total magnetic moments of Fe_nPt_{55-n} nanoparticles. Considering the influence of different location of Pt atom on the magnetic moment, we calculate the total magnetic moment of Fe_{55} nanoparticle when the Fe atom at the center(C) site, 1st shell (1S) site, the edge of the vertex in 2nd shell (ET) site, the top of the vertex in 2nd shell (VT) site was substituted by Pt atom, respectively. The isomer $Fe_{54}Pt_{1C}$ nanoparticle with one Pt substitution at the center site has the maximum magnetic moment of 148.08 μ_B, which is higher than that of Fe_{55} nanoparticle (145.29 μ_B). With one Pt substitution at the 1S site, the magnetic moment of the isomer $Fe_{54}Pt_{1S}$ nanoparticle is 141.28 μ_B. While the Fe atom at the VT site is substituted by the Pt atom, the magnetic moment of the isomer $Fe_{54}Pt_{1VT}$ nanoparticle decreases to

Table 4
The position of the Fe atom with the maximum or minimum atomic magnetic moment: the center (C), 1 st shell (1S), the edge of the vertex in second shell (ET), the top of the vertex in second shell (VT). Pt-c (Fe-c) represents that the center of the nanoparticles is occupied by Pt (Fe) atom.

Nanoparticles	$m_L(\mu_B)$			
	Fe_{max}	Position	Fe_{min}	Position
Fe_9Pt_{46} (Pt-c)	3.35	ET	2.93	VT
$Fe_{11}Pt_{44}$(Fe-c)	3.29	ET	2.43	C
$Fe_{13}Pt_{42}$(Pt-c)	3.28	ET	3.03	1S
$Fe_{19}Pt_{36}$(Fe-c)	3.31	ET	2.56	C
$Fe_{22}Pt_{33}$(Fe-c)	3.20	ET	2.30	C
$Fe_{27}Pt_{28}$(Pt-c)	3.16	ET	2.66	1S
$Fe_{33}Pt_{22}$(Fe-c)	3.07	ET	−1.86	C
$Fe_{36}Pt_{19}$(Fe-c)	3.11	ET	2.04	C
$Fe_{42}Pt_{13}$(Fe-c)	3.03	ET	−1.49	C
$Fe_{44}Pt_{11}$(Fe-c)	2.96	ET	0.72	C
$Fe_{46}Pt_9$(Pt-c)	2.90	ET	2.08	1S

120.46 μ_B. The isomer $Fe_{54}Pt_{1ET}$ nanoparticle has the minimum magnetic moment (101.45 μ_B) with one Pt substitution at the ET site. From the results, we deduce that the total magnetic moments of Fe_nPt_{55-n} nanoparticles are sensitive to the substitution position of Pt atom.

In order to explore the origin of the effect of Pt position on magnetic moment, DOS of the Fe_{55}, $Fe_{54}Pt_{1C}$, $Fe_{54}Pt_{1S}$, $Fe_{54}Pt_{1ET}$, and $Fe_{54}Pt_{1VT}$ nanoparticles are exhibited in Fig. 7. From Fig. 7(a), we find that there are some overlapping peaks between Fe-3*d* orbital and Pt-3*d* orbital in the energy −2.0 to 2.0 eV, which implies a strong interaction between Fe-3*d* and Pt-5*d* orbitals. Because of this interaction, we can clearly see that the peak at the −0.5 to 0.0 eV for spin up orbital shifts to the low energy levels in the total density of states. Close to the Fermi level, the exchange splitting is 2.47 eV for $Fe_{54}Pt_{1C}$ nanoparticle, which is larger than that of Fe_{55} nanoparticle (2.36 eV). Therefore, the magnetic moment of $Fe_{54}Pt_{1C}$ nanoparticle is larger than that of Fe_{55} nanoparticle by 2.79 μ_B. In $Fe_{54}Pt_{1S}$ nanoparticle, the overlapping peaks of Fe-3*d* and Pt-5*d* in the energy −2.0 to 2.0 eV reduce and the exchange splitting is 2.25 eV, as shown in Fig. 7(b). The magnetic moment of $Fe_{54}Pt_{1S}$ nanoparticle decreases slightly. In $Fe_{54}Pt_{1ET}$ and $Fe_{54}Pt_{1VT}$ nanoparticles, the symmetry of Pt-5*d* orbital increases and the peaks of Fe-3*d* orbital slightly overlap the peaks of the Pt-5*d* in the energy 0.0 to 2.0 eV, which leads to the peaks of spin up orbitals at −0.5 to 0.5 eV cross the Fermi surface and shift to the high energy levels in the TDOS, and the peaks of spin down orbitals at the 1.0 to 2.0 eV shift to the low energy levels in Fig. 7(c) and (d). The value of the exchange splitting in $Fe_{54}Pt_{1VT}$ and $Fe_{54}Pt_{1ET}$ nanoparticles decreases to 1.63 and 1.11 eV, respectively. The magnetic moments of $Fe_{54}Pt_{1VT}$, $Fe_{54}Pt_{1ET}$ nanoparticles rapidly decrease to 120.46 and 101.45 μ_B. Therefore, the Pt atom at the center site has promotion effect on the total magnetic moments of the Fe_nPt_{55-n} nanoparticles, while at the sublayer and outmost layer has inhibition effect.

To further understand the influence of different location of Pt atom on the magnetic moment, we also calculate the magnetic moments of $Fe_{13}@Pt_{42}$, $Fe_{12}Pt_{43}$ ($L1_0$), $Fe_{43}Pt_{12}$ ($L1_0$) and $Fe_{42}@Pt_{13}$ nanoparticles, as also presented in Table 1. With the Pt atoms occupying the outmost layer and one Pt substitution at the center site, the total magnetic moment of $Fe_{12}Pt_{43}$ ($L1_0$) nanoparticle is higher than that of $Fe_{13}@Pt_{42}$ nanoparticles by 0.18 μ_B. When the Pt atoms occupy the sublayer, with one Pt substitution at the center site, the total magnetic moment of $Fe_{42}@Pt_{13}$ nanoparticle is higher than that of $Fe_{43}Pt_{12}$ ($L1_0$) nanoparticle by 5.3 μ_B. This characteristic indicates that the inhibition effect of the outmost layer Pt atoms is stronger than that of the sublayer Pt atoms.

Because the position of the atoms has a great effect on the magnetic moment, we calculate the atomic magnetic moment for the every Fe atom, and analyze the position of the Fe atom with the maximum or minimum atomic magnetic moment, as listed in Table 4. We find that the Fe atom at the ET site has the maximum atomic magnetic moment, while at the center site has minimum atomic magnetic moment. When the center site is occupied by the Pt atom, the Fe atom at the 1S or VT site has the minimum atomic magnetic moment. Therefore, if we want to increase the total magnetic moment of Fe_nPt_{55-n} nanoparticles, the Fe atom should be put at the ET site as much as possible and the one Pt atom should occupy the center site.

4. Conclusion

In summary, we use DFT calculation to study the structural, electronic and magnetic properties of Fe_nPt_{55-n} nanoparticles. For Fe_nPt_{55-n} nanoparticles, the positive E_{seg} of Fe indicates that Fe tends to occupy the center site and the negative E_{seg} of Pt proves that Pt prefers to occupy surface sites. As a result, the surface Pt fraction is larger than surface Fe fraction in Fe_nPt_{55-n} nanoparticles. There exists a relationship between the surface Fe fraction and excess energy that the smaller of the surface Fe fraction and the lower of the excess energy are, the higher stability of Fe_nPt_{55-n} nanoparticles is. $Fe_{13}@Pt_{42}$ nanoparticle with the smallest surface Fe fraction and the lowest excess energy is the most stable structure among all the icosahedral Fe_nPt_{55-n} nanoparticles. Though the analysis of Bader charge and difference charge density, we obtain that Fe atom transfers charge to Pt atom and charge transfer reaches the maximum when the atomic ratio of Fe and Pt is 1:1. The total magnetic moments of Fe_nPt_{55-n} nanoparticles increase with the increasing of Fe composition. The analysis of DOS indicates that exchange splitting increases with the increasing of Fe composition, which leads to the increase of magnetic moments. The total magnetic moments of Fe_nPt_{55-n} nanoparticles are also sensitive to the substitution position of Pt atom. With one Pt atom substituted at the center site, Pt-5*d* orbitals will interact with Fe-3d orbitals, boosting the exchange splitting. As a result, the total magnetic moments of $Fe_{54}Pt_{1C}$ nanoparticles increase. The Pt atom at the center site has promotion effect on the total magnetic moment of the Fe_nPt_{55-n} nanoparticles. Similarly, when the Fe atom in the 1S, ET or VT site is substituted by Pt atom, the total magnetic moments of the Fe_nPt_{55-n} nanoparticles decrease. Pt atom in the sublayer and outmost layer has inhibition effect on the total magnetic moment of the Fe_nPt_{55-n} nanoparticles, and the inhibition effect of the outmost layer Pt atoms are stronger than those of the sublayer Pt atoms. At different position, the atom also has the different atomic magnetic moment. Fe atom at the ET site has the largest atomic magnetic moment, and at the center site has minimum atomic magnetic moment. Therefore, we can put the Fe atom at the ET site as much as possible and put one Pt atom at the center site to increase the total magnetic moments of Fe_nPt_{55-n} nanoparticles.

Acknowledgement

This work is supported by the National Natural Science Foundation of China (Grant No. 21376013).

Appendix A. Supplementary data

Supplementary data associated with this article can be found, in the online version, at http://dx.doi.org/10.1016/j.jmgm.2015.10.010.

References

[1] L.H. He, J. Li, Y.J. Wang, A.L. Wang, W. Zhen, J.C. Chen, L.Y. Chen, S.Y. Wang, Z.C. Shen, The magnetic and magneto-optical properties of PtFe–Co multiulayers, Mater. Sci. Eng. B 76 (2000) 43–46.

[2] T. Katayama, T. Sugimoto, Y. Suzuki, M. Hashimoto, P. de Haan, J.C. Lodder, Magneto-optical Kerr rotation spectra in ordered and disordered phases of Fe–Pt alloy films, J. Magn. Magn. Mater. 104–107 (Part 2) (1992) 1002–1004.
[3] M. Kumar, T. Nautiyal, S. Auluck, Magneto-optical properties of transition metal compounds XPt_3 (X = V, Cr, Mn, Fe, Co) and X_3Pt (X = Fe, Co), J. Alloys Compd. 486 (2009) 60–65.
[4] E.E. Shalyguina, K.-H. Shin, Oscillatory behaviour of magnetic and magneto–optical properties in Fe–Pt thin-film structures, J. Alloys Compd. 326 (2001) 298–302.
[5] A. Fortunelli, A.M. Velasco, Structural and electronic properties of Pt/Fe nanoclusters from EHT calculations, J. Mol. Struct.: THEOCHEM 487 (1999) 251–266.
[6] A.R. Malheiro, J. Perez, H.M. Villullas, Dependence on composition of electronic properties and stability of Pt–Fe/C catalysts for oxygen reduction, J. Power Sources 195 (2010) 7255–7258.
[7] Y.-H. Chung, D.Y. Chung, N. Jung, H.-Y. Park, Y.-E. Sung, S.J. Yoo, Effect of surface composition of Pt–Fe nanoparticles for oxygen reduction reactions, Int. J. Hydrogen Energy 39 (2014) 14751–14759.
[8] A. Fortunelli, A.M. Velasco, A theoretical study of the catalytic properties of Pt/Fe nanoclusters, J. Mol. Struct.: THEOCHEM 586 (2002) 17–27.
[9] L. Guczi, K. Matusek, M. Eszterle, Preparation, characterization, and catalytic activity of silica-supported highly dispersed Pt–Fe catalysts, J. Catal. 60 (1979) 121–132.
[10] M. Kotobuki, A. Watanabe, H. Uchida, H. Yamashita, M. Watanabe, High catalytic performance of Pt–Fe alloy nanoparticles supported in mordenite pores for preferential CO oxidation in H_2-rich gas, Appl. Catal. A 307 (2006) 275–283.
[11] W. Li, Q. Xin, Y. Yan, Nanostructured Pt–Fe/C cathode catalysts for direct methanol fuel cell: the effect of catalyst composition, Int. J. Hydrogen Energy 35 (2010) 2530–2538.
[12] X. Liu, O. Korotkikh, R. Farrauto, Selective catalytic oxidation of CO in H_2: structural study of Fe oxide-promoted Pt/alumina catalyst, Appl. Catal. A 226 (2002) 293–303.
[13] A.R. Malheiro, J. Perez, H.M. Villullas, Surface structure and electronic properties of Pt–Fe/C nanocatalysts and their relation with catalytic activity for oxygen reduction, J. Power Sources 195 (2010) 3111–3118.
[14] L. Ou, The origin of enhanced electrocatalytic activity of Pt–M (M = Fe, Co, Ni, Cu, and W) alloys in PEM fuel cell cathodes: a DFT computational study, Comput. Theor. Chem. 1048 (2014) 69–76.
[15] T. Tamaki, A. Minagawa, B. Arumugam, B.A. Kakade, T. Yamaguchi, Highly active and durable chemically ordered Pt–Fe–Co intermetallics as cathode catalysts of membrane–electrode assemblies in polymer electrolyte fuel cells, J. Power Sources 271 (2014) 346–353.
[16] H. Zhang, D. Lin, G. Xu, J. Zheng, N. Zhang, Y. Li, B.H. Chen, Facile synthesis of carbon supported Pt-nanoparticles with Fe-rich surface: a highly active catalyst for preferential CO oxidation, Int. J. Hydrogen Energy 40 (2015) 1742–1751.
[17] W. Yu, M.D. Porosoff, J.G. Chen, Review of Pt-based bimetallic catalysis: from model surfaces to supported catalysts, Chem. Rev. 112 (2012) 5780–5817.
[18] F. Tao, S. Zhang, L. Nguyen, X. Zhang, Action of bimetallic nanocatalysts under reaction conditions and during catalysis: evolution of chemistry from high vacuum conditions to reaction conditions, Chem. Soc. Rev. 41 (2012) 7980.
[19] R. Ferrando, J. Jellinek, R.L. Johnston, Nanoalloys: from theory to applications of alloy clusters and nanoparticles, Chem. Rev. 108 (2008) 845–910.
[20] J. Jellinek, Nanoalloys: tuning properties and characteristics through size and composition, Faraday. Discuss. 138 (2008) 11–35.
[21] N. Toshima, T. Yonezawa, Bimetallic nanoparticles-novel materials for chemical and physical applications, New J. Chem. 22 (1998) 1179–1201.
[22] C.N. He, N.Q. Zhao, One-step solid-phase synthesis of ultrasmall homogeneous face-centered tetragonal FePt nanoparticles encapsulated in thin carbon shells, J. Mater. Chem. 22 (2012) 1297–1304.
[23] S. Sun, Recent advances in chemical synthesis, self-assembly, and applications of FePt nanoparticles, Adv. Mater. 18 (2006) 393–403.
[24] Ch.V. Rao, B. Viswanathan, ORR activity and direct ethanol fuel cell performance of carbon-supported Pt–M (M = Fe Co and Cr) alloys prepared by polyol reduction method, J. Phys. Chem. C 113 (2009) 18907–18913.
[25] A.K. Shukla, R.K. Raman, N.A. Choudhury, K.R. Priolkar, P.R. Sarode, S. Emura, R. Kumashiro, Carbon-supported Pt–Fe alloy as a methanol-resistant oxygen-reduction catalyst for direct methanol fuel cells, J. Electroanal. Chem. 563 (2004) 181–190.
[26] F.-J. Lai, H.-L. Chou, L.S. Sarma, D.-Y. Wang, Y.-C. Lin, J.-F. Lee, B.-J. Hwang, C.-C. Chen, Tunable properties of Pt_xFe_{1-x} electrocatalysts and their catalytic activity towards the oxygen reduction reaction, Nanoscale 2 (2010) 573–581.
[27] L.A.W. Green, N.T.K. Thanh, High pressure synthesis of FePt nanoparticles with controlled morphology and Fe content, RSC Adv. 4 (2014) 1168–1173.
[28] K. Boufala, L. Fernández-Seivane, J. Ferrer, M. Samah, Magnetic properties of Fe_{2n} and $(FePt)_n (n \leq 5)$ clusters and magnetic anisotropy of transition metal dimers, J. Magn. Magn. Mater. 322 (2010) 3428–3437.
[29] J. Habeeb Mokkath, Nanometer size 3d–4d and 3d–5d substitutional clusters: promising candidates for magnetic storage applications, J. Magn. Magn. Mater. 334 (2013) 31–35.
[30] J. VandeVondele, M. Krack, F. Mohamed, M. Parrinello, T. Chassaing, J. Hutter, QUICKSTEP: fast and accurate density functional calculations using a mixed gaussian and plane waves approach, Comput. Phys. Commun. 167 (2005) 103–128.
[31] G. Lippert, J. Hutter, M. Parrinello, A hybrid Gaussian and plane wave density functional scheme, Mol. Phys. 92 (1997) 477–487.
[32] J.P. Perdew, K. Burke, M. Ernzerhof, Generalized gradient approximation made simple, Phys. Rev. Lett. 77 (1996) 3865–3868.
[33] S. Goedecker, M. Teter, J. Hutter, Separable dual-space Gaussian pseudopotentials, Phys. Rev. B 54 (1996) 1703–1710.
[34] J. VandeVondele, J. Hutter, Gaussian basis sets for accurate calculations on molecular systems in gas and condensed phases, J. Chem. Phys. 127 (2007) 114105.
[35] G. Kresse, J. Furthmüller, Efficient iterative schemes for ab initio total-energy calculations using a plane-wave basis set, Phys. Rev. B 54 (1996) 11169–11186.
[36] J.A. Alonso, Electronic and atomic structure, and magnetism of transition-metal clusters, Chem. Rev. 100 (2000) 637–678.
[37] F. Baletto, R. Ferrando, Structural properties of nanoclusters: energetic, thermodynamic, and kinetic effects, Rev. Mod. Phys. 77 (2005) 371–423.
[38] F. Baletto, R. Ferrando, A. Fortunelli, F. Montalenti, C. Mottet, Crossover among structural motifs in transition and noble-metal clusters, J. Chem. Phys. 116 (2002) 3856–3863.
[39] N. Toshima, H. Yan, Y. Shiraishi, Recent progress in bimetallic nanoparticles: their preparation, structures and functions, in: B. Corain, G. Schmid, N. Toshima (Eds.), Metal Nanoclusters in Catalysis and Materials Science: the Issue of Size Control, Elsevier, Amsterdam, 2008, pp. 49–75.
[40] F. Zhao, C. Liu, P. Wang, S. Huang, H. Tian, First-principles investigations of the structural electronic and magnetic properties of $Pt_{13-n}Ni_n$ clusters, J. Alloys Compd. 577 (2013) 669–676.
[41] M.J. Piotrowski, P. Piquini, J.L.F. Da Silva, Platinum-based nanoalloys Pt_nTM_{55-n}(TM = Co, Rh, Au): a density functional theory investigation, J. Phys. Chem. C 116 (2012) 18432–18439.
[42] A.I. Frenkel, Applications of extended X-ray absorption fine-structure spectroscopy to studies of bimetallic nanoparticle catalysts, Chem. Soc. Rev. 41 (2012) 8163–8178.
[43] M.R. Knecht, M.G. Weir, A.I. Frenkel, R.M. Crooks, Structural rearrangement of bimetallic alloy PdAu nanoparticles within dendrimer templates to yield core/shell configurations, Chem. Mater. 20 (2008) 1019–1028.
[44] S. Blundell, Magnetism in Condensed Matter, Oxford Univ. Press, 2001.